HHS Public Access

Author manuscript

Mol Imaging Biol. Author manuscript; available in PMC 2016 April 29.

Published in final edited form as:

Mol Imaging Biol. 2011 February ; 13(1): 140–151. doi:10.1007/s11307-010-0308-y.

[(Methyl)1-^{11}C]-Acetate Metabolism in Hepatocellular Carcinoma

Nicolas Salem[1], **Yu Kuang**[1], **David Corn**[2], **Bernadette Erokwu**[2], **Jeffrey A. Kolthammer**[1], **Haibin Tian**[2], **Chunying Wu**[2], **Fangjing Wang**[1], **Yanming Wang**[1,2], and **Zhenghong Lee**[1,2]

[1]Department of Biomedical Engineering, Case Western Reserve University, Cleveland, OH 44106, USA

[2]Department of Radiology, University Hospitals Case Medical Center, Cleveland, OH 44106, USA

Abstract

Purpose—Studies have established the value of [(methyl)1-^{11}C]-acetate ([^{11}C]Act) combined with 2-deoxy-2[^{18}F]fluoro-D-glucose (FDG) for detecting hepatocellular carcinoma (HCC) using positron emission tomography (PET). In this study, the metabolic fate of [^{11}C]Act in HCC was characterized.

Methods—Experiments with acetic acid [1-^{14}C] sodium salt ([^{14}C]Act) were carried out on WCH-17 cells and freshly derived rat hepatocytes. PET scans with [^{11}C]Act were also carried out on woodchucks with HCC before injection of [^{14}C]Act. The radioactivity levels in different metabolites were quantified with thin-layer chromatography.

Results—In WCH-17 cells, the predominant metabolite was phosphatidylcholine (PC). Regions of HCCs with the highest [^{11}C]Act uptake had higher radioactivity accumulation in lipid-soluble compounds than surrounding hepatic tissues. In those regions, PC and triacylglycerol (TG) accumulated more radioactivity than in surrounding hepatic tissues.

Conclusions—High [^{11}C]Act uptake in HCC is associated with increased *de novo* lipogenesis. PC and TG are the main metabolites into which the radioactive label from [^{11}C]Act is incorporated in HCC.

Keywords

Acetate; Hepatocellular carcinoma (HCC); Positron emission tomography (PET); Liver cancer; Tumor metabolism; Lipid; Woodchuck; *Marmota monax*

Introduction

Hepatocellular carcinoma (HCC) is the 5th/8th most common cancer and the 3rd/6th deadliest cancer among men/women, respectively [1]. The World Health Organization estimates that by 2030, liver cancer will account for 1.4% of all deaths worldwide, ranking 13th among the leading causes of death [2]. The incidence of HCC has doubled in North America over recent decades (between 1976 and 1995), primarily because of an increase in

Correspondence to: Zhenghong Lee; zxl11@case.edu.

Nicolas Salem and Yu Kuang equally contributed to the work presented in this manuscript.

hepatitis C virus infection [3, 4]. Despite advances in the characterization of the disease and the development of new therapeutic agents, the 5-year survival rate in the USA is still only 6%, with a median survival of 7 months [5]. One of the reasons for the low survival rate is that HCC is often asymptomatic in its early stages. When patients start showing symptoms, the tumor has spread and/or grown beyond the point at which it can be surgically removed and other less successful therapeutic strategies have to be considered. Globally, the median survival rate is 3 months when HCC is clinically diagnosed, but 85% of the patients can be cured with early diagnostic and intervention [6]. This highlights the importance of improving detection methods and developing technologies to facilitate research on new treatments.

The reported sensitivity of positron emission tomography (PET) with 2-deoxy-2[^{18}F]fluoro-D-glucose (FDG) for detecting HCC is less than ideal, ranging between 40% and 65% [7–12]. Along with the costs and limited availability of PET scanners in some regions, this explains why FDG-PET is not recommended in the management of patients with HCC [13, 14]. Current research efforts are focused on evaluating other PET radiotracers for improved detection of lesions in the liver. Recently, [(methyl)1-^{11}C]-acetate ([^{11}C] Act) was shown to be more sensitive than FDG for PET imaging of HCC in humans, detecting between 78% and 87% of the tumors [15–18]. These studies have demonstrated that FDG and [^{11}C]Act complement each other, with [^{11}C]Act accumulating preferentially in well-differentiated tumors and FDG accumulating preferentially in poorly-differentiated tumors, and that the accumulation of FDG in HCC correlated with poor prognosis [17]. When patients were imaged with both FDG and [^{11}C]Act, more than 85% of the HCCs showed increased uptake of at least one radiotracer. [^{11}C]Act is suspected to be metabolized through the tricarboxylic acid (TCA) cycle and converted to lipids in HCC, but its exact metabolic profile remains to be characterized.

An estimated 80% of all HCC cases worldwide are etiologically associated with chronic hepatitis B (HepB) infection [19]. The woodchuck hepatitis virus (WHV), a member of the *Hepadnaviridae* family, is similar in structure, genetic organization, and life cycle to the human HepB virus. When infected at birth, woodchucks (*Marmota monax*) can develop chronic hepatitis infection which will almost always progress to HCC by the age of 4 years [20]. The woodchuck therefore provides an animal model of hepatocarcinogenesis occurring on a background of chronic inflammation induced by hepatitis virus infection. In contrast with xenograft models, the etiology, influence of the micro-environment, and involvement of different cell types can be studied. As such, this animal model has been extensively used to study the process of hepatocarcinogenesis [21–26]. Immunization procedures, nucleoside analogs, and antiviral therapies were also evaluated on woodchucks chronically infected with WHV [27–31]. We have previously quantified the pharmacokinetics of FDG in the woodchuck model of HCC and demonstrated that increased FDG uptake was observed in a subset of tumors with higher FDG uptake than the surrounding hepatic tissues (four out of ten). These tumors had a decreased k_4/k_3 ratio (which has been reported elsewhere to correlate with the glucose 6-phosphatase to hexokinase activity ratio [32]) compared to the surrounding liver tissues and were moderately differentiated [33]. We then semiquantitatively assessed Act for imaging HCC on this animal model and showed that, like in human studies, well-differentiated tumors had increased Act uptake and moderately-

to poorly-differentiated tumors had increased FDG uptake compared with the surrounding hepatic tissues [34]. Per lesion analysis also showed that, while FDG detected only seven out of 13 HCCs, Act detected 16 out of 17 HCCs. In this study, we characterized the metabolic fate of [^{11}C]Act in a cell line derived from an adult woodchuck hepatoma and in woodchuck tumors and surrounding liver tissues.

Materials and Methods

Chemicals and Reagents

Acetic acid [1-^{14}C] sodium salt ([^{14}C]Act) dissolved in saline was obtained from American Radiolabeled Chemicals, Inc. (St. Louis, MO, USA). Cholesterol (CHO), sphingomyelin, L-α-phosphatidylcholine (PC), L-α-phosphatidylethanolamine (PE), L-α-phosphatidyl-DL-glycerol (PG), L-α-phosphatidylinositol, L-α-phosphatidylserine (PS), L-α-phosphatidic acid (PA), 1-oleoyl-2-hydroxy-*sn*-glycero-3-phosphocholine (lysophosphatidylcholine), and 1,2-dioleoyl-*sn*-glycerol (1,2-DAG) were obtained from Avanti Lipids (Alabaster, AL, USA). L-Alanine (A), L-cysteine (C), L-cystine (CN), L-aspartic acid (D), L-glutamic acid (E), glycine (G), L-histidine (H), L-asparagine (N), L-proline (P), L-glutamine (Q), L-arginine (R), L-serine (S), L-tyrosine (Y), cholesteryl oleate, sodium palmitate and sodium oleate, mono-, di (1,2- and 1,3-DAG)-, and triglyceride (TG) mix, Percoll® and fetal bovine serum (FBS) were obtained from Sigma-Aldrich (St. Louis, MO, USA). Ninhydrin, primulin, high-performance liquid chromatography-grade methanol, chloroform, water, glacial acetic acid, ethyl ether anhydrous, acetone, hexanes, potassium hydroxide, perchloric acid, *sec*-butanol, and 100 mm culture dishes coated with rat tail collagen I were obtained from Thermo Fisher Scientific (Waltham, MA, USA). Bio-Safe II scintillation counting cocktail was obtained from Research Products International Corp. (Mount Prospect, IL, USA). Dulbecco's modified Eagle medium (DMEM) containing 4.5 mg/l of D-glucose, 2 mM L-glutamine, and 110 mg/l of sodium pyruvate, DMEM/F12 containing 15 mM of 4-(2-hydroxyethyl)-1-piperazineethanesulfonic acid buffer and 2 mM L-glutamine, penicillin (10,000 U)–streptomycin (10,000 μg; liquid), William's medium E, hepatocyte wash medium, liver perfusion medium, liver digest medium, Hepato-ZYME-SFM, Dulbecco's phosphate-buffered saline (DPBS) containing calcium and magnesium, trypan blue stain, and Leibovitz's L-15 medium were obtained from Invitrogen (Carlsbad, CA, USA). Permafluor® E^{+} and Carbo-Sorb® E were obtained from Perkin-Elmer (Waltham, MA, USA).

Cell Lines and Animals

WCH-17 cells derived from a WHV-induced hepatoma in an adult woodchuck were obtained from American Type Culture Collection (Manassas, VA, USA). WCH-17 cells were seeded at a density of 1×10^{7}cells per 100-mm-diameter culture dish and maintained in DMEM supplemented with 10% FBS and 5% penicillin–streptomycin at 37°C in a humidified atmosphere of 90% air and 10% CO_2. The cells were used 24 h after plating (Fig. 1a). Two adult male Sprague Dawley®™ SD®™ rats weighing between 250 and 300 g were obtained from Harlan (Indianapolis, IN, USA). Three woodchucks with HCC weighing 2.5, 2.2, and 3.2 kg were obtained from Northeastern Wildlife (Harrison, ID, USA). These woodchucks were wild-caught and screened for HCC by serological testing for WHV and

liver enzymes. Twelve hours before the imaging experiments, the woodchucks were fasted; otherwise, they had access to water and food (Teklad Laboratory Diets for Rodents, Harlan; Madison, WI, USA) per normal husbandry. The animals used in this study were treated in accordance with the guidelines and recommendations of the Institutional Animal Care and Use Committees of Case Western Reserve University (Cleveland, OH, USA).

Derivation of a Primary Rat Hepatocytes Cell Line

A perfusion-collagenase method for the derivation of a cell line from a rat liver was described by Berry and Friend [35]. A modified version of the original protocol was implemented in this study. Briefly, anesthesia was induced in Sprague–Dawley rats with ketamine and xylazine (60:5 mg/kg) injected intramuscularly. The rats were placed in dorsal recumbency on a heating pad in which 37°C water was circulated by a Gaymar T/Pump (Gaymar; Orchard Park, NY, USA). The abdomen was shaved and the area was sterilized with iodine. A 2-in. incision was made on the ventral midline, and the viscera were exposed by cutting along the linea alba and through the peritoneal membrane. The viscera were displaced and an 18-gauge catheter was inserted in the superior mesenteric vein and pushed into the portal vein. The vena cava was cut as warm liver perfusion medium (37°C) supplemented with 10 ml of penicillin–streptomycin was circulated at a rate of 30 ml/ min for 15 min. This was immediately followed by a collagenase– dispase digestion with warm liver digest medium (37°C) at 30 ml/ min for another 15 min. The liver was then aseptically removed to a conical tube containing 15 ml of cold L-15 medium. The hepatocytes were released by gentle stirring, and the cell suspension was centrifuged at 60×*g* for 5 min at 4°C. The supernatant was removed and the pellet was resuspended in cold hepatocyte wash medium supplemented with 5 ml of penicillin–streptomycin and filtered with 70 μm Nylon cell strainers (BD Falcon™; Bedford, MA, USA). The cell suspension was washed twice in cold hepatocyte wash medium supplemented with 5 ml of penicillin–streptomycin. The hepatocytes were purified by centrifugation at 1,300×*g* for 5 min at 4°C in a Percoll solution with a density of 1.08 g/ml. Trypan blue exclusion assay confirmed a viability exceeding 95%. The hepatocytes were seeded in 100-mm-diameter cell culture dishes coated with rat tail collagen type I at a density of 4×10^6 cells per dish in 10 ml of William's medium E supplemented with 1% penicillin–streptomycin and 5% FBS. The cells were incubated at 37°C in a humidified atmosphere of 90% air and 10% CO_2. Four hours after plating, the culture medium was removed and replaced with 10 ml of HepatoZYME-SFM supplemented with 1% penicillin–streptomycin and 2 mM of L-glutamine (Fig. 1b). The hepatocytes were used 24 h after plating (Fig. 1c).

Pulse-Chase and Incubation Experiments

Pulse-chase experiments were designed to characterize the dynamics of [^{14}C]Act metabolism in WCH-17 cells and in normal rat hepatocytes. For the pulse, the culture medium from each dish was replaced with 10 ml of DMEM/F12 containing 185 kBq of [^{14}C] Act, and the cells were incubated at 37°C in a ventilated container within the incubator. After 5 min, the medium was removed and the cells were rinsed once with 10 ml of DMEM/F12 containing 9.09 μM of unlabeled acetate. This process required less than 3 min to perform. The cells were then chased with DMEM/F12 containing 9.09 μM of unlabeled acetate for 10, 25, 40, and 55 min at 37°C in the same ventilated container. Cells

were also incubated in DMEM/ F12 with 37 kBq of [^{14}C]Act at 37°C for 5, 15, 30, 45, and 60 min in a ventilated container. After the chase or incubation, the medium was removed and the cells were rinsed once with 10 ml of cold DPBS. The media from the chase, incubation, and from the rinsing were collected for further analysis. To each culture dish, 1.2 ml of cold water was added before the cells were scraped off and collected in a glass tube. The cell mixture was then homogenized on ice for 3 min using an Omni Tissue Homogenizer (Omni International; Marietta, GA, USA). One hundred microliters of the homogenate was taken for determining the protein content according to the Bradford method, and another 100 µl of the homogenate was taken for determining the total radioactivity uptake [36]. For the experiments with hepatocytes, 0.25 mg of protein was subtracted from the total protein content to account for the collagen coating the culture dishes.

^{14}C-CO_2 Measurements

The ^{14}C-CO_2 generated as a result of [^{14}C]Act metabolism in rat hepatocytes and in WCH-17 cells was measured in two steps. First, the evaporated ^{14}C-CO_2 was measured as follows: the container within the incubator had a small hole in the lid and could accommodate three culture dishes at a time. The air from the container was bubbled through 30 ml of Carbo-Sorb® E in a Buchner flask. A vacuum pump connected to the Buchner flask was used to circulate the air from the container through the Carbo-Sorb® E. After the pulse, chase, or incubation, the Carbo-Sorb® E was separated into three vials and 10 ml of Permafluor® E$^+$ was added to each vial before scintillation counting. Second, the soluble carbon dioxide (present in the form of CO_2, carbonic acid, bicarbonate, and carbonate) was released by acidifying the media from the pulse, chase, or from the incubation (including rinsing media) with 5 ml of 12.1 M chloridric acid in a sealed system overnight. The ^{14}C-CO_2 released was trapped in 10 ml of Carbo-Sorb® E in a glass vial within a sealed system, and 10 ml of Permafluor® E$^+$ was added before scintillation counting. To derive the total ^{14}C-CO_2 generated by the cells in one culture dish at a given time point, the measured ^{14}C-CO_2 dissolved in the media produced by these cells was added to the evaporated ^{14}C-CO_2.

Lipid Extraction

A method for separating the water- and lipid-soluble fractions from cell suspensions or tissue homogenates was described by Bligh and Dyer [37]. This technique was applied to separate insoluble and water- and lipid-soluble compounds immediately after the pulse-chase and the incubation experiments in normal rat hepatocytes and in WCH-17 cells. The insoluble compounds were kept for separating the RNA, DNA, and proteins. The solvents of the water-and lipid-soluble fractions were evaporated under a stream of nitrogen gas. The dried water-soluble compounds were redissolved in 0.5 ml of 95% ethanol and 0.5% chloridric acid, and the dried lipid-soluble compounds were redissolved in 0.5 ml chloroform/ methanol (2:1 *v*/*v*). One hundred-microliter aliquots from both fractions were mixed with 5 ml Bio-Safe II for determining the total radioactivity content with scintillation counting.

RNA, DNA, and Protein Separation

The method described by Smillie and Krotkov was applied to the insoluble phase remaining after the tissue extraction procedure to separate the RNA, DNA, and proteins [38]. Each fraction was mixed with 5 ml Bio-Safe II before scintillation counting.

Water-Soluble Metabolites

Most of the radioactivity from [^{14}C]Act in the water-soluble fraction of different cancer cell lines was previously shown to be within amino acids [39]. Therefore, thin-layer chromatography (TLC) on glass plates coated with 0.25-mm-thick silica gel G 60 F254 with a preconcentration zone (Merck; Darmstadt, Germany) was used to separate the amino acids as described by Norfolk *et al.* [40]. The mobile phase consisted of sec-butanol, water, and acetic acid (3:1:1 *v*/*v*). Ten microliters from each sample was spotted in the concentration zone at the bottom of the TLC plate, and samples were eluted until the solvent front reached 17 cm (~6 h). The plates were then dried overnight and exposed to Molecular Dynamics storage phosphor screens for 1 week before being read on a GE Typhoon™ 9200 scanner (General Electric Healthcare; Piscataway, NJ, USA). Volume analysis of the bands was performed using ImageQuant™ TL 7.0 (General Electric Healthcare; Piscataway, NJ, USA; Fig. 2b). The retention factor (R_f) calculated as the ratio of the distance traveled by a compound and the distance traveled by the solvent front was automatically computed for each compound. After exposing the screen, the plate was sprayed with ninhydrin to identify amines (Fig. 2b). The approximate R_f for amino acids are listed in Table 1.

Lipid-Soluble Metabolites

TLC on glass plates coated with 0.25-mm-thick silica gel G 60 F254 with a preconcentration zone (Merck; Darmstadt, Germany) was also used to separate the lipid-soluble metabolites. However, two different mobile phases were used to separate polar and nonpolar lipids [41]. Ten microliters from each sample was spotted in the concentration zone and first developed in chloroform, methanol, and water solution (60:30:5 *v*/*v*) until the solvent front reached 7 cm. The plate was then dried and developed again in hexanes, ethyl ether anhydrous, and acetic acid (80:20:1.5 *v*/*v*) until the solvent front reached 17 cm. The plate was dried before spraying with a primulin solution (5 mg in 100 ml of acetone and water; 80:20 *v*/*v*) for identifying lipids under ultraviolet (UV) light (Fig. 2a). The different ^{14}C-labeled lipids were identified using the nonradiolabeled standards. Quantification of the radioactivity content in each metabolite was carried out as described above. The approximate R_f for the different lipids are listed in Table 1.

PET Imaging Studies

[^{11}C]Act was produced from [^{11}C]CO_2, which resulted in the ^{11}C label in C-1 position using Grignard reagent [42]. Prior to imaging, the three woodchucks were anesthetized with an intramuscular injection of 5 mg/kg of xylazine and 50 mg/kg of ketamine. Thereafter, incremental injections of pentobarbital were used to maintain anesthesia. Intravascular injections of a bolus of 37 MBq [^{11}C]Act were administered in each animal, and 60-min scans were acquired on a Gemini TF PET/CT scanner (Philips Medical Systems; Cleveland, OH, USA). Dynamic data from list-mode acquisition were rebinned into a total of 44 frames

(6×5, 6×10, 6×30, 6×60, 4×90, 4×120, 4× 180, 6×300, and 2×500 s), and the 3D emission scans were reconstructed using row-action maximum likelihood algorithm (two iterations, relaxation factor=0.045 and blob size=2.5 pixels). CT attenuation correction was used. All reconstructed PET images were 144×144 pixels, for a field-of-view diameter of 576 mm, yielding a voxel size of 4×4×4 mm. After imaging, the woodchucks were kept under anesthesia with pentobarbital, which was administered as needed. A 29.6-MBq bolus of [^{14}C]Act was injected in the same vein used for [^{11}C]Act injection within 20 min after the end of the PET scan. The three woodchucks were euthanized using FatalPlus (Vortech Pharmaceuticals, Ltd.; Dearborn, MI, USA) 15, 30, and 60 min after [^{14}C]Act injection, respectively.

Tissue Extraction and Metabolites Analysis

Immediately after euthanasia, the liver was examined to determine the number of macroscopic HCCs and each tumor was grossly sectioned. Different regions of the tumors were classified according to their visual appearance on the reconstructed PET images (at the same time point at which the animal was euthanized). HCC_{Low} had lower or similar [^{11}C]Act uptake compared with the surrounding hepatic tissues. $HCC_{Moderate}$ had higher [^{11}C]Act uptake than the surrounding hepatic tissues, and HCC_{High} were the regions of maximum uptake in the tumors and had greater [^{11}C]Act uptake than the surrounding hepatic tissues. Multiple samples weighing approximately 0.2 g were obtained from liver tissues surrounding the tumors and from different HCC regions, a procedure which took at approximately 15 min. Each sample was homogenized in 1 ml of water for 3 min on ice with an Omni Tissue Homogenizer (Omni International; Marietta, GA, USA). One hundred microliters of homogenate was mixed with 5 ml of Bio-Safe II, and the total tissue radioactivity content was measured by scintillation counting. Another 100 μl was collected to determine the tissue protein content using the Bradford method [36]. Lipids were separated from nonlipid compounds following the Folch method [43]. The water- and lipid-soluble fractions were gently dried with a stream of nitrogen gas and redissolved as described above. One hundred-microliters aliquots were mixed with 5 ml Bio-Safe II for scintillation counting of the radioactivity content in both fractions. The lipid- and water-soluble metabolites were separated with TLC and quantified as described above.

Statistical Analysis

Each *in vitro* experiment was carried out in triplicate, and the results are reported as average ± standard deviation. Significant differences between the radioactivity retained in the insoluble and lipid- and water-soluble fractions were determined by a two-tailed unpaired *t* test with unequal variance. The *P* values were calculated with Origin 8 (version 8.0987), and a significance level of 0.05 was used. The standardized uptake value (SUV) calculated as the radioactivity concentration within a region of interest (ROI) normalized by the ratio of the injected dose, and the animal weight was used as a semiquantitative measure of [^{11}C]Act distribution in different regions of the liver or HCCs on the PET images. ROIs with a diameter of 1.2 cm were drawn over the areas of maximum [^{11}C]Act uptake on the PET images and on the liver tissues adjacent to the HCCs to determine the SUV_{HCC}/SUV_{Liver}. The largest dimension of each tumor was reported as the tumor diameter.

Results

In vitro Studies

Rat hepatocytes and WCH-17 cells were incubated for different durations with [^{14}C]Act before the nature of the radioactive metabolites was investigated (Fig. 3). For both cell types, the total radioactivity content in the collected cells increased with the duration of the incubation. However, the total radioactivity retained into WCH-17 cells was higher than that in rat hepatocytes for incubation durations longer than 5 min ($P \leq 0.002$). In WCH-17 cells, the levels of ^{14}C in the lipid-soluble fraction were higher than the levels of ^{14}C in the water-soluble fraction for incubation durations longer than 15 min ($P \leq 0.01$). In rat hepatocytes, except for the 60-min incubation duration, the ^{14}C content in lipid-soluble metabolites was lower than that in water-soluble metabolites ($P \leq 0.003$). The rate of conversion of [^{14}C]Act to [^{14}C]CO_2 was not significantly different between the two cell lines ($P \geq 0.18$). TLC was used to separate the water- and the lipid-soluble metabolites retained in rat hepatocytes and in WCH-17 cells. In rat hepatocytes, the predominant metabolites were TG, 1,2-DAG, and CHO, some amino acids (D, G, Q, P, and S), and A, accounting for 16.1%, 15.7%, 13.4%, and 11% of the total retained radioactivity after a 60-min incubation period, respectively. In WCH-17 cells, the predominant metabolites were PC, A, and some amino acids (D, G, Q, P, and S), accounting for 27.3%, 16.3%, and 12.2% of the total retained radioactivity after a 60-min incubation duration, respectively.

Pulse-chase experiments with [^{14}C]Act were also carried out on the same cell lines to observe transient trends in the metabolism of [^{14}C]Act (Fig. 4). In rat hepatocytes, the total radioactivity retained rapidly fell by 74% with a 10-min chase and remained low with longer chase durations. The decrease in the total radioactivity content in WCH-17 cells was more progressive as it only fell by 42% with a 55-min chase. Accordingly with the rapid drop in total retained radioactivity, the production of ^{14}C-CO_2 by rat hepatocytes stabilized by 10 min after the beginning of the chase whereas the levels of radioactive ^{14}C-CO_2 steadily increased with increasing chase durations in WCH-17 cells. The radioactivity content in water-soluble compounds decreased with increasing chase durations in rat hepatocytes and in WCH-17 cells. In both cell types, the radioactivity content in lipid-soluble compounds increased with increasing chase durations of up to 25 min. The levels of radioactivity in lipid-soluble compounds were higher than those into water-soluble compounds with a 40-min chase in rat hepatocytes ($P = 0.03$) and with 25-, 40-, and 55-min chases in WCH-17 cells ($P \leq 0.04$). TLC was also used to separate the water- and lipid-soluble metabolites of [^{14}C] Act in each experiment. In rat hepatocytes, the predominant metabolites were 1,2-DAG and CHO, PC, and TG, each of which accounted for 26.8%, 20.9%, and 19.5% of the total retained radioactivity with a 55-min chase, respectively. In WCH-17 cells, PC, A, and proteins contained 26.5%, 11.4%, and 11.2% of the total retained radioactivity with a 55-min chase, respectively, and were the predominant metabolites.

In vivo Studies

Woodchuck #1 had a single 8.2-cm tumor with heterogeneous radioactivity distribution and a SUV_{HCC}/SUV_{Liver} of 1.15 (15 min after [^{11}C]Act injection; average SUV in a region near the maximum; Fig. 5a). This animal was injected with [^{14}C]Act after PET imaging and

euthanized 15 min postinjection (p.i.). Three samples from liver tissues surrounding the tumors (liver), three from regions of the HCC with [^{11}C]Act uptake similar to the surrounding hepatic tissues (HCC_{Low}), and four from areas of the HCC with moderate [^{11}C]Act uptake ($HCC_{Moderate}$) were collected for analysis. The radioactivity content in the lipid-soluble fraction of $HCC_{Moderate}$ was higher than that of liver (P=0.02; Fig. 5b). The radioactivity content in the water-soluble fraction and in insoluble material was not significantly different among HCC_{Low}, $HCC_{Moderate}$, and liver (P>0.05). Woodchuck #2 had a single 6.5-cm tumor with a SUV_{HCC}/ SUV_{Liver} of 2.42 (30 min after [^{11}C]Act injection; average SUV in a region near the maximum; Fig. 5d). This animal was injected with [^{14}C]Act after PET imaging and euthanized 30 min p.i.. Seven samples from liver tissues surrounding the tumors (liver), two from regions of the HCC with moderate [^{11}C]Act uptake ($HCC_{Moderate}$), and eight from areas of the HCC with high [^{11}C]Act uptake (HCC_{High}) were collected for analysis. The total radioactivity content in $HCC_{Moderate}$ and HCC_{High} was higher than that in liver (P<0.001; Fig. 5e). The ^{14}C levels in lipid-soluble compounds and insoluble materials were also higher in HCC_{High} (P< 0.001). The tumor in woodchuck #3 was 2.3 cm in diameter, and it had a SUV_{HCC}/SUV_{Liver} of 1.47 (60 min after [^{11}C] Act injection; average SUV in a region near the maximum; Fig. 5g). This animal was injected with [^{14}C]Act after PET imaging and euthanized 60 min p.i.. Three samples from liver tissues surrounding the tumors (liver), two from regions of the HCC with [^{11}C]Act uptake similar to the surrounding hepatic tissues (HCC_{Low}), and three from areas of the HCC with high [^{11}C]Act uptake (HCC_{High}) were collected for analysis. The total ^{14}C content of HCC_{High} was higher than that of liver (P=0.002; Fig. 5h). Incorporation of ^{14}C into lipid-soluble compounds was higher in HCC_{High} compared to the surrounding hepatic tissues (P=0.01). The levels of ^{14}C in water-soluble compounds were not significantly different in liver, in HCC_{Low}, and in HCC_{High} (P>0.05). Significantly more of the radioactivity was found in the insoluble fraction in HCC_{High} compared to liver (P=0.001).

In woodchuck #1, the ^{14}C content in any metabolites was not significantly different in HCC_{Low} and liver (P>0.06; Fig. 5c). Among the metabolites which accounted for more than 10% of the total radioactivity content in $HCC_{Moderate}$, PC (22.6%), PE (10.7%), and TG (16.6%) incorporated significantly more of the radioactivity from [^{14}C]Act than liver (P≤0.04). In the liver tissues of woodchuck #2, most of the radioactivity was found in N (16.7%), RNA (14%), D, G, Q, P, and S (11.6%), A (10.9%), and proteins (10.4%; Fig. 5f). In $HCC_{Moderate}$, TG and PC contained 38.3% and 13.8% of the total radioactivity, respectively. Only PC contained more than 10% of the total radioactivity content in $HCC_{Moderate}$ and accumulated significantly more of the radioactivity from [^{14}C]Act than in liver (P=0.02). In HCC_{High}, 32.1%, 19.7%, and 10.5% of the total ^{14}C was found in TG, PC, and 1,2-DAG and CHO, respectively. The ^{14}C levels were significantly higher in these three metabolites when compared to those in liver (P<0.001). The radioactivity content of any metabolites was similar in liver and HCC_{Low} in woodchuck #3 (P90.05; Fig. 5i). Only PC, which accounted for more than 10% of the total radioactivity in HCC_{High} (14.3%), had increased ^{14}C contained compared to PC in liver (P=0.01).

Discussion

[^{11}C]Act is known to be predominantly metabolized to CO_2 through the TCA cycle in the myocardium [44]. Although it has been suspected to be incorporated predominantly in lipids, the metabolic pathway(s) responsible for [^{11}C]Act uptake and retention in liver tumors was unknown. The metabolism of [^{14}C]Act was characterized in four different human cancer cell lines (nasal septum, ovary, colon, and skin) and compared with that in fibroblasts [39]. [^{14}C]Act incorporation into lipids was shown to correlate with growth activity, and compared with fibroblasts, the levels of radioactive PC were higher in tumor cell lines. In this study, *in vitro* experiments were carried out to observe the dynamics of [^{14}C]Act and to allow a comparison of the fraction of [^{14}C]Act oxidized through the TCA cycle to ^{14}C-CO_2 relative to that metabolized through anabolic pathways. Because hepatocytes account for nearly 80% of the liver parenchymal volume and represent the cell type in which most of the metabolism takes place, a woodchuck hepatoma-derived cell line and a freshly derived rat hepatocytes cell line were used [45]. The results showed that WCH-17 cells incorporate more ^{14}C from [^{14}C]Act into lipids, water-soluble, and insoluble compounds compared with rat hepatocytes. Pulse-chase experiments also showed increased production of ^{14}C-CO_2 by WCH-17 cells. In these cancerous cells, the ^{14}C label from [^{14}C]Act was found in several metabolic species, the predominant one being PC, accounting for approximately 27% of the total retained radioactivity after a 60-min incubation or 55-min chase. In rat hepatocytes, although the radioactivity was mostly distributed among PC, 1,2-DAG and CHO, and TG, these species only incorporated 67.1% and 40.9% of the ^{14}C in the 55-min chase and 60-min incubation experiments, respectively. These findings are in agreement with the results obtained in other human cancer cell lines [39].

Interspecies differences between rats and woodchucks might have affected the levels of radioactivity derived from radiolabeled acetate incorporated into different metabolites. However, when looking at the comparisons between WCH-17 and rat hepatocytes and between woodchuck HCCs and surrounding liver tissues, several similarities were observed. First, similar to what was observed *in vivo*, the total radioactivity retained by rat hepatocytes at any time point is less than that retained by WCH-17 cells. Second, in both rat hepatocytes and liver tissues surrounding the tumors, metabolism of radiolabeled acetate into water-soluble compounds dominated over that in lipid-soluble compounds whereas the opposite was seen in WCH-17 cells or in HCC_{High}. Third, incorporation of the ^{14}C label from ^{14}C-Act into insoluble compounds (RNA, DNA, or proteins) was lower than into water- or lipid-soluble compounds in rat hepatocytes or in woodchuck liver tissues surrounding the tumors. Fourth, similar patterns of radioactivity accumulation into PC, 1,2-DAG and CHO and TG were shown in rat hepatocytes and in woodchuck liver tissues surrounding the tumors. These similarities lead us to conclude that there was no reason to believe interspecies differences between rat and woodchucks significantly affected the metabolic trends in Act metabolism in hepatocytes.

PET imaging with [^{11}C]Act was performed on three woodchucks with HCC. Analysis of the radioactive metabolites from [^{14}C]Act in different cancerous and noncancerous liver tissues was also carried out to investigate the metabolic differences which explain the contrast between liver tumors and the surrounding hepatic tissues seen on the PET images. The

results showed that PC and TG were the predominant metabolites in regions of HCC with moderate or high [^{11}C]Act uptake, accounting for up to 22.6% and 38.3% of the retained radioactivity, respectively. In one woodchuck, the levels of ^{14}C-TG were similar in regions of the HCC with high [^{11}C]Act uptake and in the surrounding liver tissues. However, consistently across all three animals, the incorporation of the ^{14}C label from [^{14}C]Act into lipids is greater in HCCs with high [^{11}C]Act uptake than in liver tissues surrounding tumors while there was no difference in the radioactivity levels in water-soluble compounds between liver tissues surrounding tumors and HCCs. Thus, the *in vitro* and *in vivo* results suggest that increased *de novo* lipogenesis in regions of some HCCs explain the contrast between the tumors and the surrounding hepatic tissues seen on the PET images.

Several human studies have demonstrated alterations in lipid metabolism in HCC. In one study, marked increases in the mRNA levels of fatty acid synthase (FAS), acetyl coenzyme A (CoA) carboxylase 1 (enzyme which synthesizes malonyl CoA from acetyl CoA), adenosine triphosphate citrate lyase (enzyme responsible for the formation of cytosolic acetyl CoA from citrate), stearoyl CoA desaturase (SCD; enzyme involved in the desaturation of saturated fatty acyl CoAs), and for the malic enzyme (enzyme catalyzing the decarboxylation of malic acid to form pyruvic acid) were measured in HCCs compared to the surrounding hepatic tissues [46]. Sterol regulatory element binding protein type 1c (SREBP-1c; a transcription factor involved in regulating the expression of lipogenic genes) expression was also higher in some HCCs. There was no clear relationship between the tumor etiology, its differentiation level, fatty change, and expression levels of lipogenic enzymes. The expression of lipogenic genes was also measured in human HCC samples and compared to noncancerous liver tissues [47]. The expression of SREBP-1c, SCD, FAS, and fatty acid desaturase 1 was significantly higher in HCCs. Another report showed that the cholesterol content in HCC samples from seven patients is higher compared with that in the surrounding liver tissues [48]. The activity of the active form of hydroxymethyl-glutaryl CoA (HMG CoA) reductase (the rate-limiting enzyme in cholesterol synthesis which produces mevalonic acid from HMG CoA) and the overall rate of cholesterol synthesis were significantly higher in these tumors. Recently, Yun *et al.* measured increased ACSS1 expression in a human HCC cell line which displayed high [^{11}C]Act uptake [49]. Finally, the tumor concentration of choline-containing compounds such as choline, phosphocholine, glycerophosphocholine, and taurine were found to be higher in the HCCs from four patients compared to the surrounding liver tissues, suggesting increased biosynthesis of membrane phospholipids [9]. Although the metabolism of radiolabeled acetate in HCC had never been characterized, these separate studies suggest that overexpression of lipogenic genes and/or increased lipogenesis often occurs in human HCC.

Oligonucleotide microarray studies were performed on HCC samples from six woodchucks and on normal liver tissues or liver tissues surrounding tumors from eight woodchucks [50]. When the woodchuck gene sequence was available, differential expression was confirmed with real-time polymerase chain reaction (RT-PCR). Among the genes which were found to be overexpressed in HCCs were SCD, elongation of long chain fatty acids (ELOVL6), diacylglycerol *O*-acyltransferase homolog 2 (enzyme which catalyzes the last step of triacylglycerol synthesis), and cytochrome P450, family 51, subfamily A, polypeptide 1 (an enzyme involved in the synthesis of cholesterol, steroids, and other lipids). Solute carrier

family 27 member 2 (a fatty acid transporter) and acetyl CoA acyltransferase 2 were among the downregulated genes. RT-PCR analysis confirmed upregulation of ACAS2 and SCD and downregulation of HMG CoA synthase. Despite the limited number of available woodchuck gene sequences and the fact that the tissues were analyzed on human microarrays, there is some agreement with the human results discussed above. ACAS activity in woodchuck HCCs was also directly assessed [51]. Results showed significantly increased ACAS activity in HCCs compared to the surrounding hepatic tissues, partially explaining the increased [^{11}C]Act uptake observed on PET images of the corresponding woodchucks. Together, these genetic profiling and enzyme activity studies support the increased [^{14}C]Act conversion into lipids (especially PC) in woodchuck HCCs observed in the current study. The exact causes of this phenomenon are still unknown and their understanding can be key in determining the value of [^{11}C]Act for detection, diagnostic, staging, or response to therapy with PET.

Conclusion

We have characterized the metabolism of [^{11}C]Act in HCC using woodchucks and showed that increased [^{11}C]Act uptake in some regions of HCC is associated with increased *de novo* lipogenesis. PC and TG are the main metabolites into which the radioactive label from [^{11}C]Act is incorporated in HCC. This knowledge can be used to assist in the development of novel therapeutics by enabling serial assessment with *in vivo* imaging.

Acknowledgments

We are grateful to Dr. Ann-Marie Broome for her technical assistance in obtaining, preserving, and maintaining the cell lines used in this study. This work was supported in part by NIH/NCI CA095307 (Principal Investigator: Zhenghong Lee), a NIH Interdisciplinary Biomedical Imaging Training Program predoctoral training grant T32EB007509-02 (Principal Investigator: David L. Wilson), and a 2008 Society of Nuclear Medicine fellowship award (recipient: Nicolas Salem). The funders had no role in study design, data collection and analysis, decision to publish, or preparation of the manuscript.

References

1. Ferlay, J.; Bray, F.; Pisani, P., et al. GLOBOCAN 2: cancer incidence, mortality and prevalence worldwide. Lyon: IARC; 2004.
2. Theakston, F., editor. World Health Statistics 2008. Geneva: World Health Organization; 2008. p. 112
3. El-Serag HB, Mason AC. Rising incidence of hepatocellular carcinoma in the United States. N Engl J Med. 1999; 340(10):745–750. [PubMed: 10072408]
4. El-Serag HB, Mason AC. Risk factors for the rising rates of primary liver cancer in the United States. Arch Intern Med. 2000; 160(21):3227–3230. [PubMed: 11088082]
5. El-Serag HB, Mason AC, Key C. Trends in survival of patients with hepatocellular carcinoma between 1977 and 1996 in the United States. Hepatology. 2001; 33(1):62–65. [PubMed: 11124821]
6. Previsani, N.; Lavanchy, D. Hepatitis B. World Health Organization—Department of Communicable Diseases Surveillance and Response. Geneva: 2002. p. 76
7. Shin JA, Park JW, An M, et al. Diagnostic accuracy of 18F-FDG positron emission tomography for evaluation of hepatocellular carcinoma. Korean J Hepatol. 2006; 12(4):546–552. [PubMed: 17237633]
8. Yamamoto Y, Nishiyama Y, Kameyama R, et al. Detection of hepatocellular carcinoma using 11C–choline PET: comparison with 18F-FDG PET. J Nucl Med. 2008; 49(8):1245–1248. [PubMed: 18632827]

9. Lin WY, Tsai SC, Hung GU. Value of delayed 18F-FDG-PET imaging in the detection of hepatocellular carcinoma. Nucl Med Commun. 2005; 26(4):315–321. [PubMed: 15753790]
10. Wudel LJ Jr, Delbeke D, Morris D, et al. The role of [18F] fluorodeoxyglucose positron emission tomography imaging in the evaluation of hepatocellular carcinoma. Am Surg. 2003; 69(2):117–124. discussion 124-116. [PubMed: 12641351]
11. Trojan J, Schroeder O, Raedle J, et al. Fluorine-18 FDG positron emission tomography for imaging of hepatocellular carcinoma. Am J Gastroenterol. 1999; 94(11):3314–3319. [PubMed: 10566736]
12. Delbeke D, Martin WH, Sandler MP, et al. Evaluation of benign vs malignant hepatic lesions with positron emission tomography. Arch Surg. 1998; 133(5):510–515. discussion 515-516. [PubMed: 9605913]
13. Bruix J, Sherman M. Management of hepatocellular carcinoma. Hepatology. 2005; 42(5):1208–1236. [PubMed: 16250051]
14. Llovet JM, Bruix J. Novel advancements in the management of hepatocellular carcinoma in 2008. J Hepatol. 2008; 48(Suppl 1):S20–S37. [PubMed: 18304676]
15. Ho CL, Yu SC, Yeung DW. 11C–Acetate PET imaging in hepatocellular carcinoma and other liver masses. J Nucl Med. 2003; 44(2):213–221. [PubMed: 12571212]
16. Li S, Beheshti M, Peck-Radosavljevic M, et al. Comparison of (11)C-acetate positron emission tomography and (67)Gallium citrate scintigraphy in patients with hepatocellular carcinoma. Liver Int. 2006; 26(8):920–927. [PubMed: 16953831]
17. Park JW, Kim JH, Kim SK, et al. A prospective evaluation of 18F-FDG and 11C-acetate PET/CT for detection of primary and metastatic hepatocellular carcinoma. J Nucl Med. 2008; 49(12):1912–1921. [PubMed: 18997056]
18. Hwang KH, Choi DJ, Lee SY, et al. Evaluation of patients with hepatocellular carcinomas using [(11)C]acetate and [(18)F]FDG PET/ CT: a preliminary study. Appl Radiat Isot. 2009; 67:1195–1198. [PubMed: 19342249]
19. Yu MC, Yuan JM, Govindarajan S, et al. Epidemiology of hepatocellular carcinoma. Can J Gastroenterol. 2000; 14(8):703–709. [PubMed: 11185536]
20. Tennant BC, Toshkov IA, Peek SF, et al. Hepatocellular carcinoma in the woodchuck model of hepatitis B virus infection. Gastroenterology. 2004; 127(5 Suppl 1):S283–S293. [PubMed: 15508096]
21. Abe K, Kurata T, Shikata T, et al. Enzyme-altered liver cell foci in woodchucks infected with woodchuck hepatitis virus. Jpn J Cancer Res. 1988; 79(4):466–472. [PubMed: 2898465]
22. Aldrich CE, Coates L, Wu TT, et al. *In vitro* infection of woodchuck hepatocytes with woodchuck hepatitis virus and ground squirrel hepatitis virus. Virology. 1989; 172(1):247–252. [PubMed: 2549713]
23. Chen HS, Kaneko S, Girones R, et al. The woodchuck hepatitis virus X gene is important for establishment of virus infection in woodchucks. J Virol. 1993; 67(3):1218–1226. [PubMed: 8437213]
24. Cote PJ, Korba BE, Steinberg H, et al. Cyclosporin A modulates the course of woodchuck hepatitis virus infection and induces chronicity. J Immunol. 1991; 146(9):3138–3144. [PubMed: 1826706]
25. Korba BE, Cote PJ, Wells FV, et al. Natural history of woodchuck hepatitis virus infections during the course of experimental viral infection: molecular virologic features of the liver and lymphoid tissues. J Virol. 1989; 63(3):1360–1370. [PubMed: 2915383]
26. Popper H, Roth L, Purcell RH, et al. Hepatocarcinogenicity of the woodchuck hepatitis virus. Proc Natl Acad Sci U S A. 1987; 84(3):866–870. [PubMed: 3468514]
27. Chu CK, Boudinot FD, Peek SF, et al. Preclinical investigation of L-FMAU as an anti-hepatitis B virus agent. Antivir Ther. 1998; 3(Suppl 3):113–121. [PubMed: 10726061]
28. Luxembourg A, Hannaman D, Wills K, et al. Immunogenicity in mice and rabbits of DNA vaccines expressing woodchuck hepatitis virus antigens. Vaccine. 2008; 26(32):4025–4033. [PubMed: 18556096]
29. Menne S, Butler SD, George AL, et al. Antiviral effect of lamivudine, emtricitabine, adefovir dipivoxil, and tenofovir disoproxil fumarate, administered orally alone and in combination, to woodchucks with chronic woodchuck hepatitis virus infection. Antimicrob Agents Chemother. 2008; 52:3617–3632. [PubMed: 18676881]

30. Menne S, Cote PJ, Korba BE, et al. Antiviral effect of oral administration of tenofovir disoproxil fumarate in woodchucks with chronic woodchuck hepatitis virus infection. Antimicrob Agents Chemother. 2005; 49(7):2720–2728. [PubMed: 15980342]
31. Menne S, Tennant BC, Gerin JL, et al. Chemoimmunotherapy of chronic hepatitis B virus infection in the woodchuck model overcomes immunologic tolerance and restores T-cell responses to pre-S and S regions of the viral envelope protein. J Virol. 2007; 81(19):10614–10624. [PubMed: 17652398]
32. Torizuka T, Tamaki N, Inokuma T, et al. *In vivo* assessment of glucose metabolism in hepatocellular carcinoma with FDG-PET. J Nucl Med. 1995; 36(10):1811–1817. [PubMed: 7562048]
33. Salem N, MacLennan GT, Kuang Y, et al. Quantitative evaluation of 2-deoxy-2[F-18]fluoro-D-glucose-positron emission tomography imaging on the woodchuck model of hepatocellular carcinoma with histological correlation. Mol Imaging Biol. 2007; 9(3):135–143. [PubMed: 17308952]
34. Salem N, Kuang Y, Wang F, et al. PET imaging of hepatocellular carcinoma with 2-deoxy-2[18F]fluoro-D-glucose, 6-deoxy-6[18F] fluoro-D-glucose, [1-11C]-acetate and [N-methyl-11C]-choline. Q J Nucl Med Mol Imaging. 2009; 53(2):144–156. [PubMed: 19039303]
35. Berry MN, Friend DS. High-yield preparation of isolated rat liver parenchymal cells: a biochemical and fine structural study. J Cell Biol. 1969; 43(3):506–520. [PubMed: 4900611]
36. Bradford MM. A rapid and sensitive method for the quantitation of microgram quantities of protein utilizing the principle of protein-dye binding. Anal Biochem. 1976; 72:248–254. [PubMed: 942051]
37. Bligh EG, Dyer WJ. A rapid method of total lipid extraction and purification. Can J Biochem Physiol. 1959; 37(8):911–917. [PubMed: 13671378]
38. Smillie RM, Krotkov G. The estimation of nucleic acids in some algae and higher plants. Can J Bot. 1960; 38:31–49.
39. Yoshimoto M, Waki A, Yonekura Y, et al. Characterization of acetate metabolism in tumor cells in relation to cell proliferation: acetate metabolism in tumor cells. Nucl Med Biol. 2001; 28(2):117–122. [PubMed: 11295421]
40. Norfolk E, Khan SH, Fried B, et al. Comparison of amino acid separations on high performance silica gel, cellulose, and C-18 reversed phase layers and application of HPTLC to the determination of amino acids in *Biomphalaria glabrata* snails. J Liq Chromatogr Relat Technol. 1994; 17(6):1317–1326.
41. Kupke IR, Zeugner S. Quantitative high-performance thin-layer chromatography of lipids in plasma and liver homogenates after direct application of 0.5-microliter samples to the silica-gel layer. J Chromatogr. 1978; 146(2):261–271. [PubMed: 212444]
42. Kihlberg T, Valind S, Langstrom B. Synthesis of [1-11C], [2-11C], [1-11C](2H3) and [2-11C](2H3)acetate for *in vivo* studies of myocardium using PET. Nucl Med Biol. 1994; 21(8):1067–1072. [PubMed: 9234364]
43. Folch J, Lees M, Sloane Stanley GH. A simple method for the isolation and purification of total lipides from animal tissues. J Biol Chem. 1957; 226(1):497–509. [PubMed: 13428781]
44. Brown M, Marshall DR, Sobel BE, et al. Delineation of myocardial oxygen utilization with carbon-11-labeled acetate. Circulation. 1987; 76(3):687–696. [PubMed: 3113765]
45. Blouin A, Bolender RP, Weibel ER. Distribution of organelles and membranes between hepatocytes and nonhepatocytes in the rat liver parenchyma. A stereological study. J Cell Biol. 1977; 72(2):441–455. [PubMed: 833203]
46. Jiang J, Xu N, Zhang X, et al. Lipids changes in liver cancer. Journal of Zhejiang University-Science B. 2007; 8(6):398–409. [PubMed: 17565510]
47. Yamashita T, Honda M, Takatori H, et al. Activation of lipogenic pathway correlates with cell proliferation and poor prognosis in hepatocellular carcinoma. J Hepatol. 2009; 50(1):100–110. [PubMed: 19008011]
48. Kawata S, Takaishi K, Nagase T, et al. Increase in the active form of 3-hydroxy-3-methylglutaryl coenzyme A reductase in human hepatocellular carcinoma: possible mechanism for alteration of cholesterol biosynthesis. Cancer Res. 1990; 50(11):3270–3273. [PubMed: 2159376]

49. Yun M, Bang SH, Kim JW, et al. The importance of acetyl coenzyme A synthetase for 11C-acetate uptake and cell survival in hepatocellular carcinoma. J Nucl Med. 2009; 50(8):1222–1228. [PubMed: 19617323]

50. Wang F, Anderson PW, Salem N, et al. Gene expression studies of hepatitis virus-induced woodchuck hepatocellular carcinoma in correlation with human results. Int J Oncol. 2006; 30(1): 33–44. [PubMed: 17143510]

51. Yu K, Schomisch SJ, Chandramouli V, et al. Hexokinase and glucose-6-phosphatase activity in woodchuck model of hepatitis virus-induced hepatocellular carcinoma. Comp Biochem Physiol C Toxicol Pharmacol. 2006; 143(2):225–231. [PubMed: 16581304]

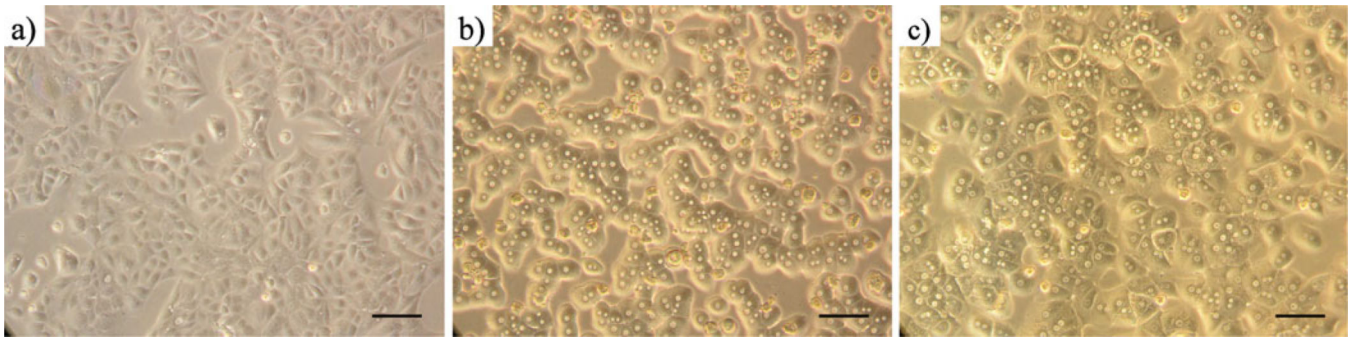

Fig. 1.

a WCH-17 cells 24 h after plating. **b** Freshly extracted rat hepatocytes 4 h after plating. **c** Rat hepatocytes 24 h after plating. Scale bar, 100 μm; original magnification ×200.

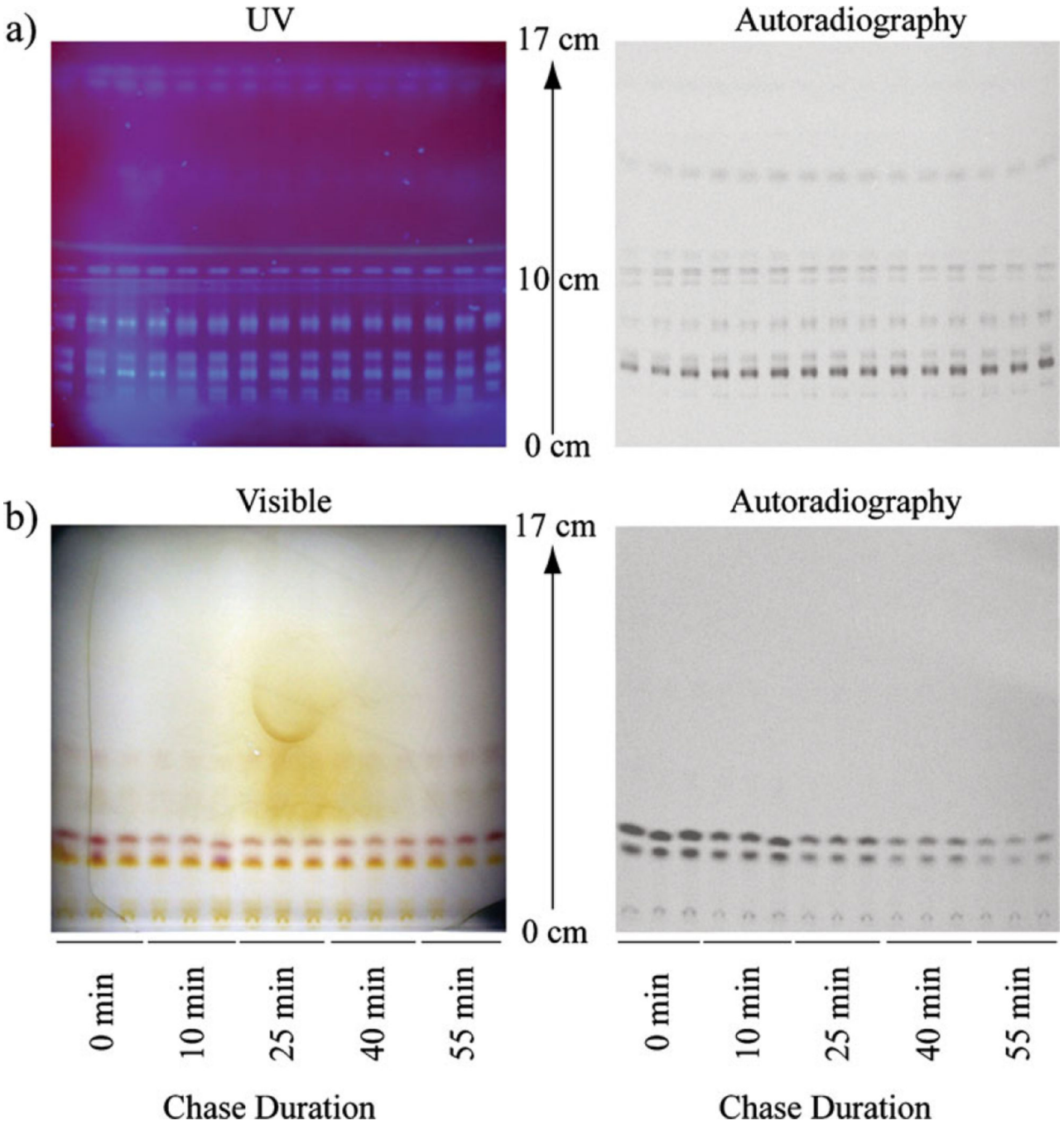

Fig. 2.

The metabolites from lipid- and water-soluble fractions were separated with TLC, visualized with either UV or visible light, and quantified with digital autoradiography. **a** Separation of the lipid-soluble metabolites from the pulse-chase experiments in WCH-17 cells. **b** Separation of the water-soluble metabolites from the pulse-chase experiments in WCH-17 cells.

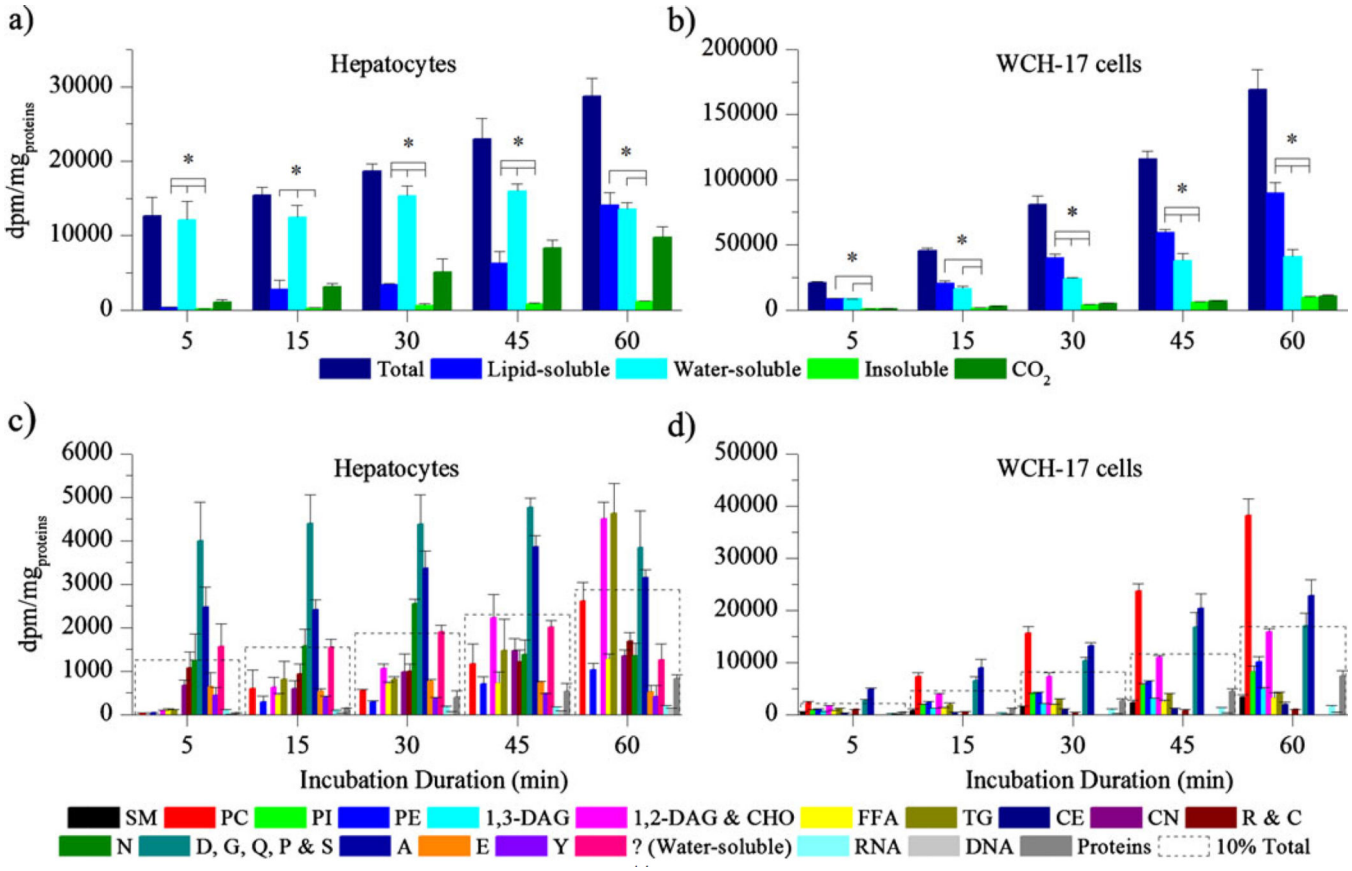

Fig. 3.

Cells were incubated for different durations with [^{14}C]Act. **a** Radioactivity content in different tissue fractions of rat hepatocytes and in CO_2. **b** Radioactivity content in different tissue fractions of WCH-17 cells and in CO_2. **c** Radioactivity content in different metabolites in rat hepatocytes. **d** Radioactivity content in different metabolites in WCH-17 cells. ? designates radioactive species of unknown nature. To put the result into perspective, a *dotted line* corresponding to 10% of the total retained radioactivity was graphed at each time point. *P<0.05.

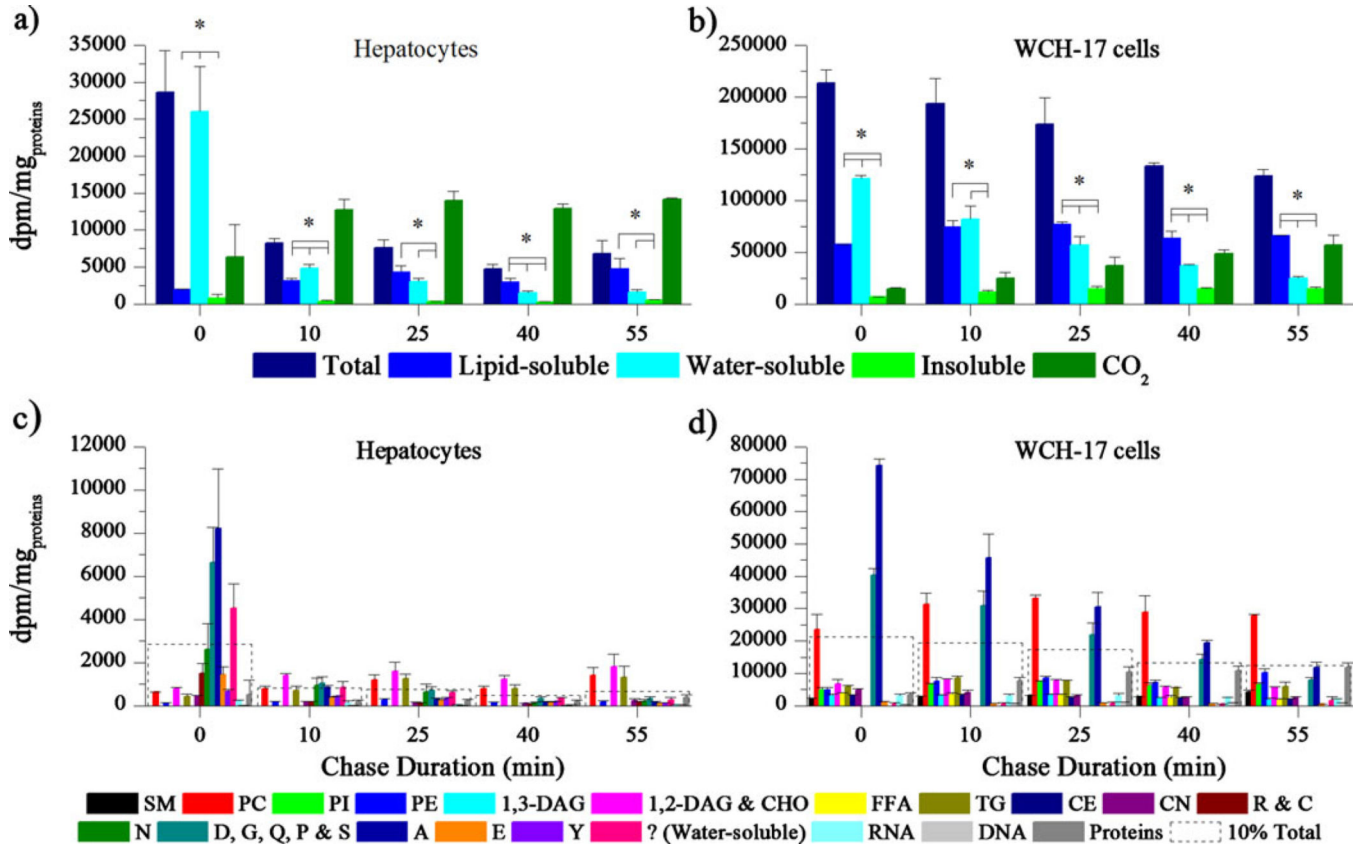

Fig. 4.

Cells were pulsed with [^{14}C]Act for 5 min and chased for different durations with the incubation medium containing unlabeled acetate. **a** Radioactivity content in different tissue fractions of rat hepatocytes and in CO_2. **b** Radioactivity content in different tissue fractions of WCH-17 cells and in CO_2. **c** Radioactivity content in different metabolites in rat hepatocytes. **d** Radioactivity content in different metabolites in WCH-17 cells. ? designates radioactive species of unknown nature. To put the results into perspective, a *dotted line* corresponding to 10% of the total retained radioactivity was graphed at each time point. *P<0.05.

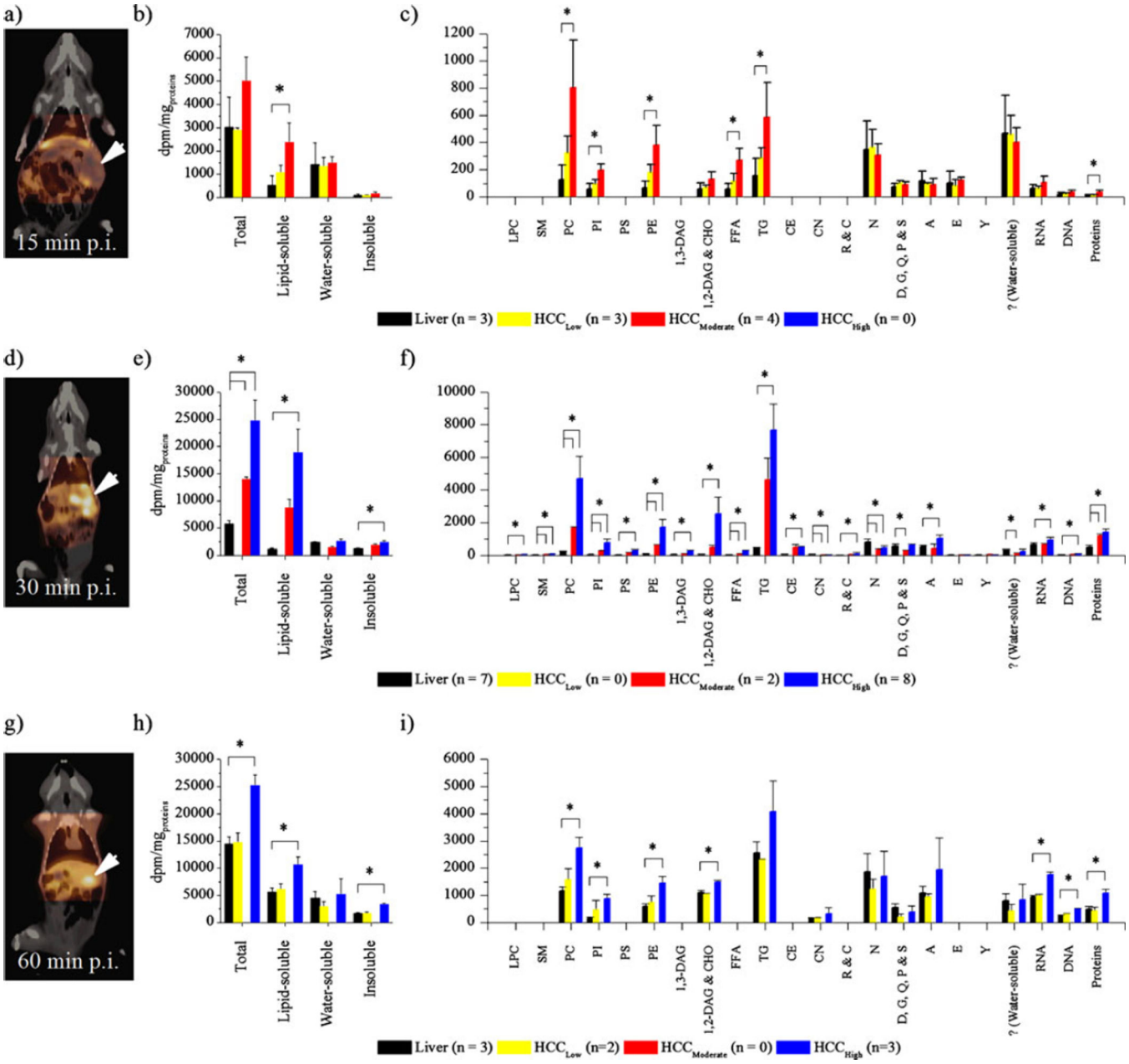

Fig. 5.

a Image of woodchuck #1 taken 15 min postinjection of [^{11}C]Act (p.i.). **b** Woodchuck #1 was euthanized 15 min p.i. of [^{14}C] Act before the radioactivity content into different tissue fractions was analyzed. **c** Radioactivity content into different metabolites in tissues of woodchuck #1. **d** Image of woodchuck #2 taken 30 min p.i. of [^{11}C]Act. **e** Woodchuck #2 was euthanized 30 min p.i. of [^{14}C]Act before the radioactivity content into different tissue fractions was analyzed. **f** Radioactivity content into different metabolites in tissues of woodchuck #2. **g** Image of woodchuck #3 taken 60 min p.i. of [^{11}C]Act. **h** Woodchuck #3 was euthanized 60 min p.i. of [^{14}C]Act before the radioactivity content into different tissue

fractions was analyzed. **i** Radioactivity content into different metabolites of woodchuck #3. ? designates radioactive species of unknown nature. *$P<0.05$.

Table 1

Approximate R_f values

Water-soluble metabolites			Lipid-soluble metabolites		
	Abbreviation	R_f		**Abbreviation**	R_f
Cystine	CN	0.05	Lysophosphatidylcholine	LPC	0.09
Histidine	H	0.06	Sphingomyelin	SM	0.13
Arginine	R	0.10	Phosphatidylcholine	PC	0.17
Cysteine	C	0.10	Phosphatidylinositol	PI	0.22
Asparagine	N	0.17	Phosphatidylglycerol	PG	0.26
Glutamine	Q	0.19	Phosphatidylserine	PS	0.28
Aspartic acid	D	0.20	Phosphatidylethanolamine	PE	0.30
Proline	P	0.20	Phosphatidic acid	PA	0.32
Glycine	G	0.21	Monoacylglycerol	MAG	0.40
Serine	S	0.23	1,3-Diacylglycerol	1,3-DAG	0.44
Alanine	A	0.26	1,2-Diacylglycerol	1,2-DAG	0.45
Glutamic acid	E	0.40	Cholesterol	CHO	0.45
Tyrosine	Y	0.44	Free fatty acids	FFA	0.49
			Triacylglycerol	TG	0.67
			Cholesterol esters	CE	0.81